Tapered N-helical metamaterials with three-fold rotational symmetry as improved circular polarizers

Johannes Kaschke,[1,*] Mark Blome,[2] Sven Burger,[2] and Martin Wegener[1]

[1] *Institute of Applied Physics, Karlsruhe Institute of Technology, 76128 Karlsruhe, Germany*

[2] *Zuse Institute Berlin, 14195 Berlin, Germany*

[*] *johannes.kaschke@kit.edu*

Abstract: Chiral helix-based metamaterials can potentially serve as compact and broadband circular polarizers. We have recently shown that the physics of structures composed of multiple intertwined helices, so called N-helices with N being an integer multiple of 4, is distinct from that of structures made of single circular helices ($N = 1$). In particular, undesired circular polarization conversion is strictly eliminated for $N = 4$ helices arranged on a square lattice. However, the fabrication of such structures for infrared/visible operation wavelengths still poses very significant challenges. Thus, we here revisit the possibility of reducing N from 4 to 3, which would ease micro-fabrication considerably. We show analytically that $N = 3$ helices arranged on a hexagonal lattice exhibit strictly vanishing circular polarization conversion. $N = 3$ is the smallest option as $N = 2$ obviously leads to linear birefringence. To additionally improve the circular-polarizer operation bandwidth and the extinction ratio while maintaining high transmission for the wanted polarization and zero conversion, we also investigate by numerical calculations $N = 3$ helices with tapered diameter along the helix axis. We find operation bandwidths as large as 2.4 octaves.

OCIS codes: (160.1585) Chiral media; (160.3918) Metamaterials; (260.5430) Polarization.

References and links

1. J. B. Pendry, "A chiral route to negative refraction," Science **306**, 1353–1355 (2004).
2. J. K. Gansel, M. Thiel, M. S. Rill, M. Decker, K. Bade, V. Saile, G. von Freymann, S. Linden, and M. Wegener, "Gold helix photonic metamaterial as broadband circular polarizer," Science **325**, 1513–1515 (2009).
3. B. Wang, J. Zhou, T. Koschny, M. Kafesaki, and C. M. Soukoulis, "Chiral metamaterials: simulations and experiments," J. Opt. A Pure Appl. Opt. **11**, 114003 (2009).
4. J. Wu, B. Ng, S. P. Turaga, M. B. H. Breese, S. A. Maier, M. Hong, A. A. Bettiol, and H. O. Moser, "Free-standing terahertz chiral meta-foils exhibiting strong optical activity and negative refractive index," Appl. Phys. Lett. **103**, 141106 (2013).
5. J. K. Gansel, M. Latzel, A. Frölich, J. Kaschke, M. Thiel, and M. Wegener, "Tapered gold-helix metamaterials as improved circular polarizers," Appl. Phys. Lett. **100**, 101109 (2012).
6. Y. Cui, L. Kang, S. Lan, S. Rodrigues, and W. Cai, "Giant chiral optical response from a twisted-arc metamaterial," Nano Lett. **14**, 1021–1025 (2014).
7. M. Li, L. Guo, J. Dong, and H. Yang, "An ultra-thin chiral metamaterial absorber with high selectivity for LCP and RCP waves," J. Phys. D: Appl. Phys. **47**, 185102 (2014).

8. K. M. McPeak, C. D. van Engers, M. Blome, J. H. Park, S. Burger, M. A. Goslvez, A. Faridi, Y. R. Ries, A. Sahu, and D. J. Norris, "Complex chiral colloids and surfaces via high-index off-cut silicon," Nano Lett. **14**, 2934–2940 (2014).
9. C. M. Soukoulis and M. Wegener, "Past achievements and future challenges in the development of three-dimensional photonic metamaterials," Nat. Photon. **5**, 523–530 (2011).
10. Z. Y. Yang, M. Zhao, P. X. Lu, and Y. F. Lu, "Ultrabroadband optical circular polarizers consisting of double-helical nanowire structures," Opt. Lett. **35**, 2588–2590 (2010).
11. Z. Y. Yang, M. Zhao, and Y. F. Lu, "Similar structures, different characteristics: Optical performances of circular polarizers with single- and double-helical metamaterials," J. Lightwave Technol. **28**, 3055–3061 (2010).
12. Z. Y. Yang, M. Zhao, and P. X. Lu, "Improving the signal-to-noise ratio for circular polarizers consisting of helical metamaterials," Opt. Express **19**, 4255–4260 (2011).
13. Z. Zhao, D. Gao, C. Bao, X. Zhou, T. Lu, and L. Chen, "High extinction ratio circular polarizer with conical double-helical metamaterials," J. Lightwave Technol. **30**, 2442–2446 (2012).
14. J. Kaschke, J. K. Gansel, and M. Wegener, "On metamaterial circular polarizers based on metal N-helices," Opt. Express **20**, 26012–26020 (2012).
15. I. Fernandez-Corbaton, "Forward and backward helicity scattering coefficients for systems with discrete rotational symmetry," Opt. Express **21**, 29885–29893 (2013).
16. Z. Lu, M. Zhao, P. Xie, L. Wu, Y. Yu, P. Zhang, and Z. Yang, "Reflection properties of metallic helical metamaterials," J. Lightwave Technol. **30**, 3050–3054 (2012).
17. P. Zhang, Z. Yang, M. Zhao, L. Wu, Z. Lu, Y. Cheng, R. Gong, Y. Zheng, and J. Duan, "Similar structures, different characteristics: circular dichroism of metallic helix arrays with single-, double-, and triple-helical structures," J. Opt. Soc. Am. A **30**, 677–681 (2013).
18. C. Menzel, C. Rockstuhl, and F. Lederer, "Advanced Jones calculus for the classification of periodic metamaterials," Phys. Rev. A **82**, 053811 (2010).
19. A. Hoop, "A reciprocity theorem for the electromagnetic field scattered by an obstacle," Appl. Sci. Res., Sect. B **8**, 135–140 (1960).
20. R. J. Potton, "Reciprocity in optics," Rep. Prog. Phys. **67**, 717 (2004).
21. R. Bhandari, "Reciprocity constraints on the matrix of reflection from optically anisotropic surfaces," J. Opt. Soc. Am. A **26**, 2368–2372 (2009).
22. J. K. Gansel, M. Wegener, S. Burger, and S. Linden, "Gold helix photonic metamaterials: a numerical parameter study," Opt. Express **18**, 1059–1069 (2010).

1. Introduction

Chiral effects like optical activity or circular dichroism require both electric and magnetic-dipole responses and are usually weak in natural substances. In contrast, in metamaterials, they can be many orders of magnitude larger [1–8] and can also be tuned to desired operation wavelengths. The status has been reviewed in [9]. In regard to concrete applications, gold-helix metamaterials have been suggested as compact and broadband circular polarizers [2] in analogy to linear wire-grid polarizers. Using a combination of direct laser writing and electroplating, high-quality structures have been fabricated for mid-infrared frequencies [2]. Both, extinction ratio and bandwidth have been further enhanced by tapering the helix radius along the helix axis [5]. These asymmetric tapered helices show different circular polarization conversions when changing the direction of propagation, making them either good circular polarizers or analyzers, depending on their orientation.

However, circular polarization conversions are often unwanted. They result from the end of the helix wire that, together with the helix axis, defines a direction in space that breaks the overall rotational symmetry. Linear birefringence is equivalent to circular polarization conversions. By intertwining several helices in one unit cell, these conversions can be eliminated [10–12]. $N = 2$ helices (untapered and tapered [13]) exhibit even more obviously an unwanted linear birefringence. $N > 2$ helix metamaterials show a completely different principle of operation because the blocked circular polarization cannot simply be reflected as in the case of arrays of single or double helices, but it must be absorbed. Absorption of the constituent metal of the helix is therefore crucial [14]. To fully eliminate circular polarization conversions it is important that N-fold rotational symmetry must be recovered not only by the structure, but also by the lattice [14, 15].

Here, we extend our previous symmetry analysis from the case of $N = 4, 8, 12, \ldots$ to the case of $N = 3, 6, 9, \ldots$ by arranging the N-helices onto a hexagonal lattice. We furthermore carry out numerical calculations for $N = 3$ varying a crucial parameter, namely the helix radius, to show that bandwidth and extinction ratio cannot be optimized simultaneously. We solve this dilemma by introducing tapered $N = 3$ helices. By increasing the opening angle of the taper, the bandwidth can be increased significantly while maintaining a high extinction ratio.

2. Symmetry and reciprocity

N-helices have been proposed several years ago [10–12], but certain constraints due to their principle of operation have only been studied later for the case of $N = 4, 8, 12, \ldots$ [14]. We have shown that the four-fold rotational symmetry strictly eliminates off-diagonal elements in the Jones transmission and reflection matrices in circular polarization basis, provided that no diffracted orders other than the two 0-th orders occur. In contrast to single-helix arrays, where the polarizer effect is achieved by reflecting the undesired circular polarization, N-helices show strictly identical reflectance for both circular polarizations. This fact, together with the conservation of energy implies strictly zero polarization effect in transmission, unless finite losses are present (or a static magnetic field is added).

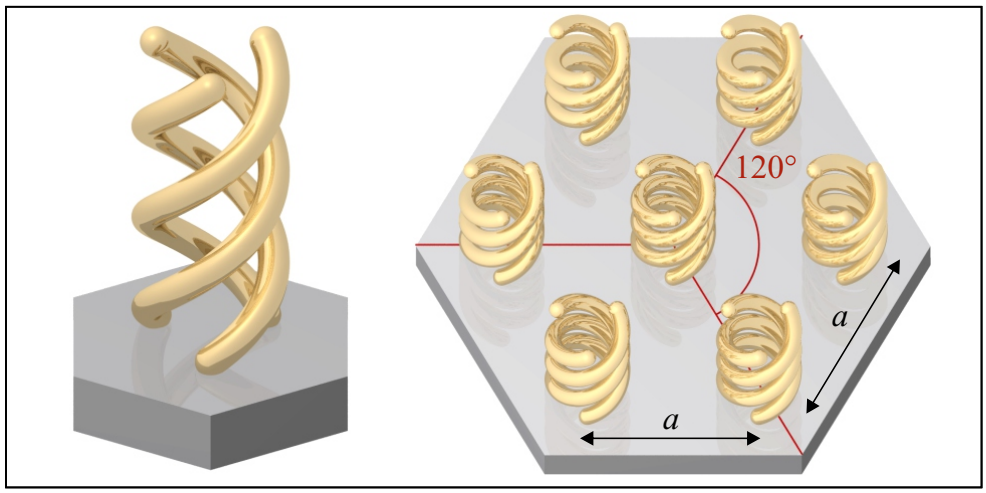

Fig. 1. The unit cell of the proposed 3-helix structure on a hexagonal lattice is shown from an oblique perspective (left). A part of the lattice is depicted on the right. The red lines are guides to the eye highlighting three-fold rotational symmetry. The distance between neighboring helices corresponds to the lattice constant a, for which we choose $a = 1\,\mu\text{m}$ throughout this article. For clarity, only a single axial pitch is depicted.

Here, we revisit the case $N = 3, 6, 9, \ldots$. While related structures and their transmittance and reflectance properties have already been studied in previous works, the underlying lattice has always been a square array [11,12,16]. This lattice does not share a common rotational symmetry with the $N = 3$ helices, hence the overall structure has only one-fold rotational symmetry. Thus, circular polarization conversion may be reduced, but it is still allowed to be finite [17].

In what follows, for the sake of simplicity, we will only explicitly address the case of $N = 3$. We do note, however, that all symmetry-based arguments also hold true for integer multiples of 3, namely $N = 3, 6, 9, \ldots$.

To fully eliminate circular polarization conversion for $N = 3$, we propose hexagonal N-helix arrays, therefore recovering three-fold rotational symmetry not only for the individual unit cell

but also for the array and therefore for the overall structure. Figure 1 shows the proposed unit cell as well as part of the lattice. Following the lines of [14], we start from the invariance of the Jones matrices for three-fold rotational symmetry under normal incidence. We assume that no diffraction orders other than the transmitted and reflected zeroth orders occur. This assumption is equivalent to stating that the lattice constant is smaller than the operating wavelength in air or in the substrate (if the structures are supported by a substrate). Furthermore, we assume that non-linear effects as well as static magnetic fields are absent. Under these conditions, the Jones reflection matrix can be written as:

$$\vec{E}_\mathrm{r} = \hat{r}_\mathrm{lin}\,\vec{E}_\mathrm{i} = \begin{pmatrix} r_\mathrm{xx} & r_\mathrm{xy} \\ r_\mathrm{yx} & r_\mathrm{yy} \end{pmatrix} \vec{E}_\mathrm{i} \tag{1}$$

We now exploit three-fold rotational symmetry, which means that the matrix $\hat{r}_\mathrm{lin}$ must be invariant under rotations of 120 degrees. Therefore, $\hat{r}_\mathrm{lin}$ has to commute with the 120-degree rotation matrix $\hat{M}_{120}$:

$$\hat{r}_\mathrm{lin} = \hat{M}_{120}\,\hat{r}_\mathrm{lin}\,\hat{M}_{120}^{-1} \tag{2}$$

In analogy to the case of $N = 4$, this also leads to $r_\mathrm{xx} = r_\mathrm{yy}$ and $r_\mathrm{yx} = -r_\mathrm{xy}$ [18]. We can hence rewrite $\hat{r}_\mathrm{lin}$:

$$\hat{r}_\mathrm{lin} = \begin{pmatrix} r_\mathrm{xx} & r_\mathrm{xy} \\ -r_\mathrm{xy} & r_\mathrm{xx} \end{pmatrix} \tag{3}$$

The same reasoning holds true for the transmission matrix $\hat{t}_\mathrm{lin}$. The basis can be changed from linear to circular polarization basis by $\hat{r}_\mathrm{circ} = \hat{S}\,\hat{r}_\mathrm{lin}\,\hat{S}^{-1}$ with the matrix $\hat{S}$ given by:

$$\hat{S} = \frac{1}{\sqrt{2}} \begin{pmatrix} 1 & -\mathrm{i} \\ 1 & \mathrm{i} \end{pmatrix} \tag{4}$$

In circular polarization we therefore get:

$$\hat{r}_\mathrm{circ} = \begin{pmatrix} r_\mathrm{RCP\ LCP} & 0 \\ 0 & r_\mathrm{LCP\ RCP} \end{pmatrix} = \begin{pmatrix} r_\mathrm{xx} + \mathrm{i}\,r_\mathrm{xy} & 0 \\ 0 & r_\mathrm{xx} - \mathrm{i}\,r_\mathrm{xy} \end{pmatrix} \tag{5}$$

and

$$\hat{t}_\mathrm{circ} = \begin{pmatrix} t_\mathrm{LCP\ LCP} & 0 \\ 0 & t_\mathrm{RCP\ RCP} \end{pmatrix} = \begin{pmatrix} t_\mathrm{xx} + \mathrm{i}\,t_\mathrm{xy} & 0 \\ 0 & t_\mathrm{xx} - \mathrm{i}\,t_\mathrm{xy} \end{pmatrix} \tag{6}$$

From here on, we could follow the same reasoning as in [14]. Instead, we follow an alternative approach that is based on a reciprocity argument. Let us first take any incoming Jones vector $\vec{a}$ which, together with the Jones matrix in forward direction $\hat{M}$ yields an emerging Jones vector $\hat{M}\vec{a}$. In the reverse direction we take a different Jones vector $\vec{b}$, the Jones matrix in reverse propagation direction $\hat{M}^\mathrm{r}$ and emerging Jones vector $\hat{M}^\mathrm{r}\vec{b}$. The De Hoop reciprocity [19–21] then states that

$$\vec{b}^{\,\dagger}\,\hat{M}\,\vec{a} = (\vec{a}^{\,*})^{\dagger}\,\hat{M}^\mathrm{r}\,\vec{b}^{\,*}, \tag{7}$$

which is satisfied provided that $\hat{M}^\mathrm{r} = \hat{M}^\mathrm{t}$, where $\hat{M}^\mathrm{t}$ denotes the transposed Jones matrix. In the special case of reflection normal to a surface, trivially, the Jones matrices in forward and reverse direction must be equal $\hat{r}_\mathrm{lin} = \hat{r}^\mathrm{r}_\mathrm{lin}$. We emphasize that $\hat{r}^\mathrm{r}_\mathrm{lin}$ does not refer to the Jones reflection from the other side of the sample, but to the Jones reflection matrix if incident and reflected field are interchanged. This leads to the general result

$$\hat{r}_\mathrm{lin} = \hat{r}^\mathrm{t}_\mathrm{lin} \tag{8}$$

The linear polarization conversions in reflection, r_{xy} and r_{yx}, must therefore be strictly equal for normal incidence: $r_{yx} = r_{xy}$.

If we now combine the restrictions for the Jones reflection matrix derived from three-fold rotational symmetry with the constraints given by reciprocity, we find that $r_{yx} = r_{xy} = 0$ and the Jones reflection matrix can be written as

$$\hat{r}_{\mathrm{lin}} = \hat{r}_{\mathrm{circ}} = \begin{pmatrix} r_{xx} & 0 \\ 0 & r_{xx} \end{pmatrix} = r_{xx}\,\mathbb{1} \tag{9}$$

The Jones reflection matrix is proportional to the identity matrix $\mathbb{1}$. Thus, the Jones reflection coefficient is the same for all polarizations. This holds true with and without losses. If, furthermore, losses are absent, conservation of energy dictates that not only the reflection coefficients but also the transmission coefficients $t_{\mathrm{RCP\ RCP}}$ and $t_{\mathrm{LCP\ LCP}}$ are equal. Therefore, without losses, any reciprocal structure posessing overall three-fold or four-fold rotational symmetry can fundamentally not act as a circular polarizer. If a polarizing effect is desired, the difference in transmittance must necessarily be achieved through absorption/losses (or, in principle, by applying an additional static magnetic field).

3. Numerical calculations

The findings of the previous section have shown a fundamentally different behavior of N-helices and single helices. While for single helices even without losses strong circular dichroism can be achieved and the undesired circular polarization is simply reflected, losses are essential for N-helices to absorb one circular polarization and transmit the other. Therefore, knowledge gained from optimizing the geometrical parameters for arrays of single helices [22] cannot be directly applied to N-helices. Here, we carry out numerical calculations using the software package JCMsuite, which is based on a frequency-domain finite-element method (FEM). Both, transmittance and reflectance spectra of electromagnetic plane waves at normal incidence have been calculated. However, as there is no difference in reflectance, only transmittance spectra are depicted. Furthermore, only the diagonal elements of the Jones matrices will be discussed because the circular polarization conversions are strictly zero. We hence only plot $T_{\mathrm{LCP}} = |t_{\mathrm{LCP\ LCP}}|^2$ and $T_{\mathrm{RCP}} = |t_{\mathrm{RCP\ RCP}}|^2$.

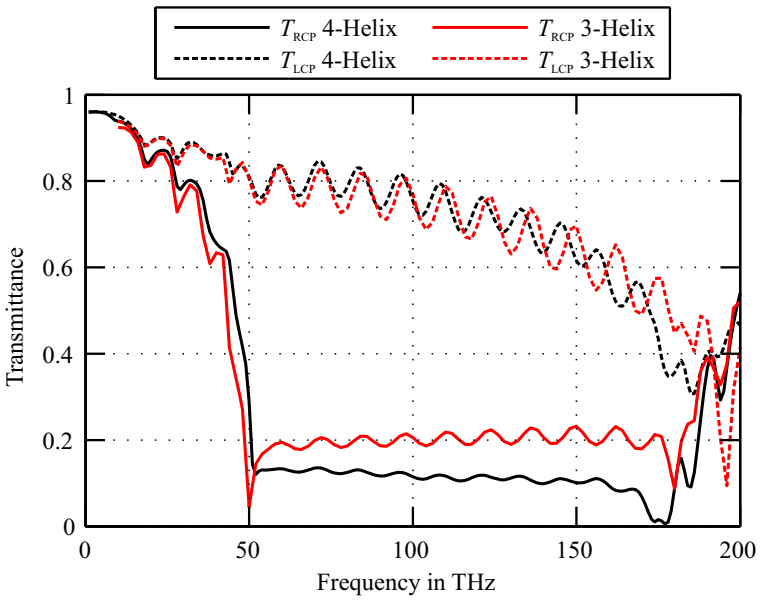

Fig. 2. Transmittance spectra for both circular polarizations are shown for $N = 4$ helices in a square array (black) and $N = 3$ helices in a hexagonal array (red) with otherwise identical geometrical parameters. Transmittance for incident right-handed circular polarization (RCP) and left-handed circular polarization (LCP) are shown by solid and dashed curves, respectively.

As a first benchmark test we have used the same geometrical parameters as before for the case of $N = 4$ helices, namely lattice period $a = 1\,\mu\text{m}$, helix radius $r_H = 300\,\text{nm}$, and wire diameter $d = 100\,\text{nm}$ [14]. Furthermore, the pitch of the helix H is chosen equal to the lateral lattice constant a. The number of helix pitches is chosen to be six in what follows (with the notable exception of Fig. 5). To obtain the optical properties of the gold helix we have used a free-electron model with a plasma frequency of $\omega_{PL} = 1.37 \times 10^{16}\,\text{rad/s}$ and a collision frequency of $\omega_{col} = 1.2 \times 10^{14}\,\text{rad/s}$. Furthermore, we have included a glass substrate in our model with a dielectric constant of $\varepsilon_{glass} = 2.25$. The lattice constant of $a = 1\,\mu\text{m}$ together with refractive index of the substrate leads to a maximum frequency $f_{max} = 200\,\text{THz}$, below which no diffraction orders other than the zeroth orders are present for light impinging along the helix axis. The calculated transmittance spectra for both cases, $N = 3$ and $N = 4$, are depicted in Fig. 2.

Clearly, the behavior is very similar in both cases. In particular, the transmittances for left-handed circularly polarized light (LCP) T_{LCP} are almost equal for $N = 3$ and $N = 4$ helices. Furthermore, the bandwidths show no significant difference. As expected, all transmittances tend to roll off for higher frequencies, simply due to the generally increasing metal absorption. All spectra exhibit fine oscillations. Intuitively, these oscillations are related to the effective modes of the system resulting from the coupling of the pitches of one helix and/or the coupling of different helices. The transmittance for right-handed circularly polarized light (RCP) T_{RCP} is higher for the case of $N = 3$ helices and only reaches values of 0.2 on average. This leads to a significantly deteriorated extinction ratio. This decrease can simply be explained by the lower effective volume filling fraction of gold as the unwanted polarization must be absorbed. This raises the question whether it is possible to find a set of geometrical parameters yielding an acceptable extinction ratio over an extended bandwidth.

One of the most crucial geometrical parameters influencing both bandwidth and extinction

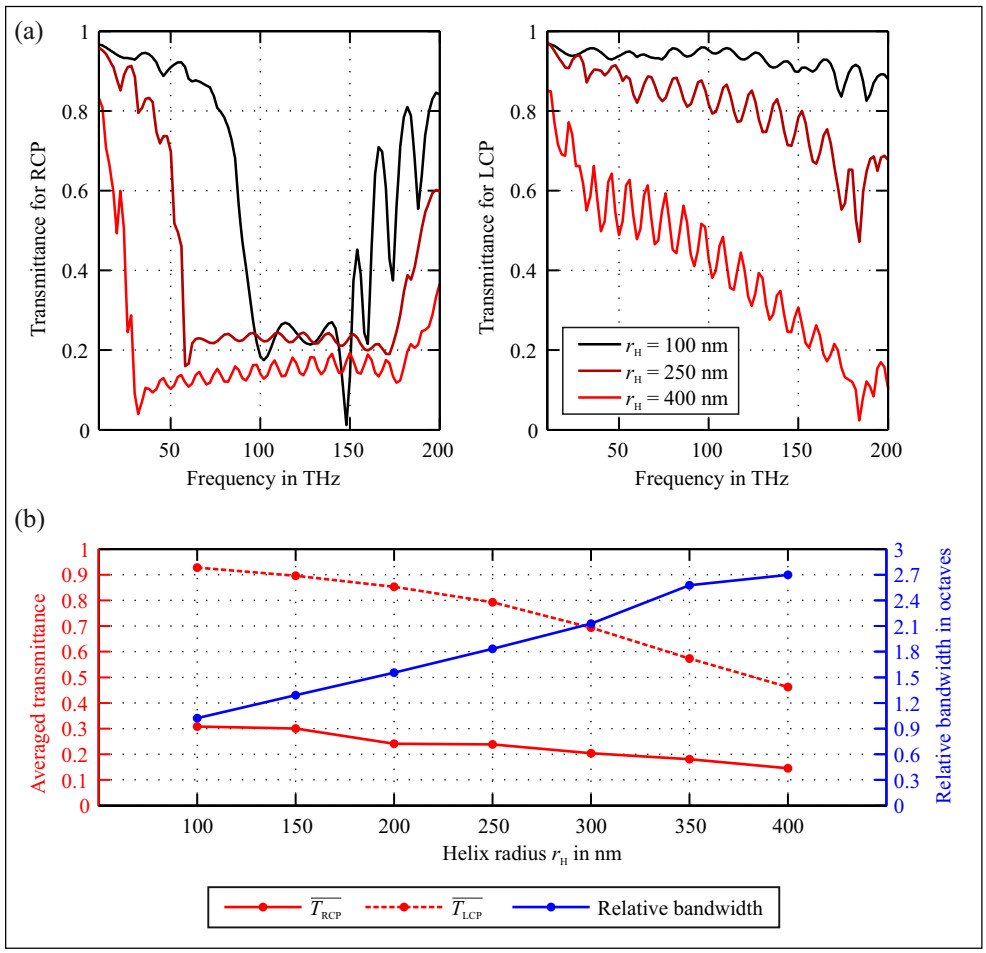

Fig. 3. The transmittance spectra for RCP and LCP are shown in (a) on the left- and right-hand side, respectively, for different helix radii r_H (color-coded). By fitting a box-function values for the relative bandwidth and average values for T_{RCP} and T_{LCP} were derived and plotted in (b).

ratio is the helix radius r_H. To optimize the optical performance of our design, we have varied the helix radius from $r_H = 100\,\text{nm}$ to $r_H = 400\,\text{nm}$. The selected, calculated spectra depicted in Fig. 3(a) show a clear trend. With increasing helix radius, the bandwidth increases significantly. Simultaneously, T_{RCP} is decreased. At first sight, this is a win-win situation. Unfortunately, however, the transmittance T_{LCP} is also decreased significantly. As can be seen from the reflectance spectra (not depicted), this decrease is mainly due to an increase in absorption. Unfortunately, due to the complexity of the system, we cannot give a simple intuitive explanation for this trend.

To deduce simple key figures to analyze these trends quantitatively, we have first normalized T_{RCP} to T_{LCP} and have then fitted a box function to extract a value for the relative bandwidth. This relative bandwidth and the two averaged transmittances $\overline{T_{LCP}}$ and $\overline{T_{RCP}}$ within the band give a total of three key figures that are plotted in Fig. 3(b) for the different helix radii. The relative bandwidth increases linearly with increasing helix radius r_H, reaching unmatched values of almost 3 octaves spanning across almost the entire mid-infrared range. The highest extinction

ratio, however, can be achieved for $r_H = 200\,\text{nm}$ with $\overline{T_{LCP}}/\overline{T_{RCP}} > 3.5$. For larger helix radii, the extinction ratio decreases again to values around $\overline{T_{LCP}}/\overline{T_{RCP}} \approx 3$. It is therefore not possible to maximize both, bandwidth and extinction ratio simultaneously.

For arrays of single helices, tapering the helix radius along the helix has previously led to a substantial improvement, both for the extinction ratio as well as for the bandwidth [5]. Therefore, we consider a tapered $N = 3$ helix structure, again arranged on a hexagonal array. The unit cell is depicted in Fig. 4(a), again only for one axial pitch for clarity. Calculations are carried out for 6 axial pitches as before. The helix radius is tapered linearly from a small radius which is kept constant at $r_H = 100\,\text{nm}$ to a large radius r_2. The orientation with respect to the substrate is not changed and always chosen as depicted. In contrast to the case of tapered single helices, for normal incidence the transmittance for a given circular polarization does not depend on the propagation direction as circular polarization conversions are zero. Only the diagonal elements of the Jones matrix are non-zero. Due to reciprocity, these have to be equal in forward and backward direction [20].

The transmittance spectra for both circular polarizations are shown in Fig. 4(b) for three selected taper ratios r_2 / r_H. The bandwidth increases considerably for large taper ratios, similarly to the untapered helix case for an increasing helix radius. The overall transmittances for both circular polarizations decrease again, but the decrease for T_{LCP} is not as pronounced as before for the case of untapered helices. This aspect leads to a higher extinction ratio.

For all calculations we have again extracted the values for relative bandwidth and averaged transmittances within the respective band. As expected, increasing the taper ratio leads to an approximately linear increase in relative bandwidth, reaching a maximum of about 2.4 octaves. The calculated bandwidth at $r_2 = 400\,\text{nm}$ is only slightly smaller than for the untapered case with $r_H = 400\,\text{nm}$. This suggests that, for N-helices, the bandwidth is mainly determined by the maximum radius of the tapered helix rather than by the tapering function.

The extinction ratio $\overline{T_{LCP}}/\overline{T_{RCP}}$, however, increases with increasing taper ratio and reaches values of $\overline{T_{LCP}}/\overline{T_{RCP}} \approx 4$ for a taper ratio of $r_2 / r_H = 4$. This trend is opposite to that observed for untapered helices.

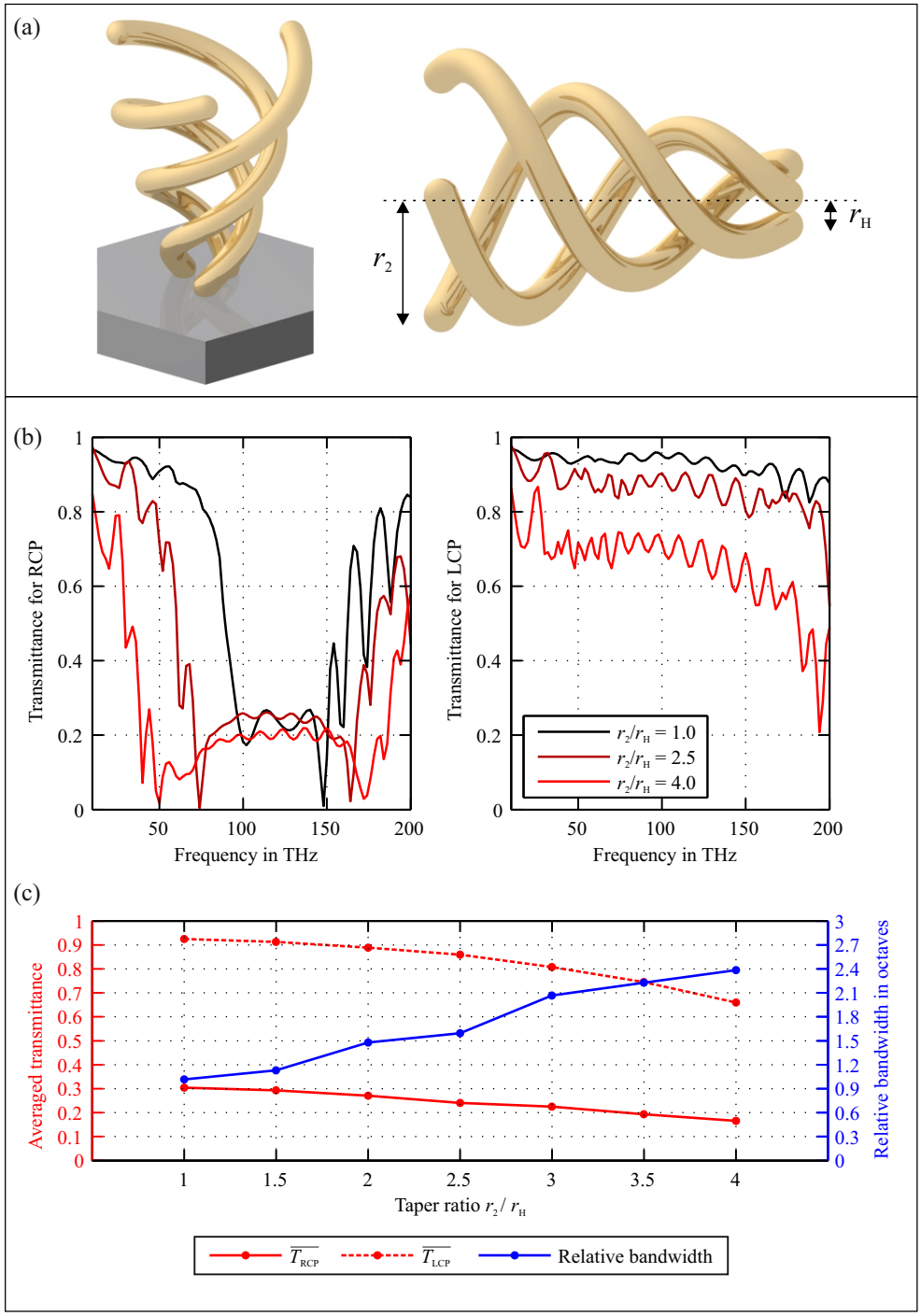

Fig. 4. (a) The unit cell of the proposed tapered $N = 3$ helix structure in a hexagonal lattice is shown from an oblique perspective (left). On the right-hand side the gold structure is depicted without the substrate from a side view to indicate r_2 and r_H. For illustration purposes only one pitch is depicted. (b) The transmittance spectra for RCP and LCP are shown on the left- and right-hand side, respectively, for selected maximum radii r_2 and therefore different taper ratios (color-coded). By fitting a box-function, values for the relative bandwidth and average values for T_{RCP} and T_{LCP} are derived and plotted in (c).

We have furthermore carried out the same calculations as above for twelve pitches. Figure 5 shows the transmittance spectra for 6 and 12 pitches for a taper ratio of $r_2 / r_H = 4$. Even though the taper angle is different, due to the different overall structure height, the change in bandwidth is negligible, suggesting that the bandwidth is only governed by the maximum radius. As expected, both transmittances T_{RCP} and T_{LCP} are decreased, but not by the same factor. Thus, the extinction ratio is increased to about $\overline{T_{LCP}}/\overline{T_{RCP}} \approx 12.5$.

For a pure bulk effect, one would expect that the transmittances for 12 pitches are simply the squares of those for 6 pitches. To allow for this comparison, we have also included the square of the transmittances for 6 pitches T_{RCP}^2 and T_{LCP}^2, depicted in gray. The calculated spectra for RCP for 12 pitches fit this expectation very well. For the case of LCP, the transmittance for 12 pitches is even higher than expected. This can probably be attributed to remaining boundary effects as well as to the different taper angle.

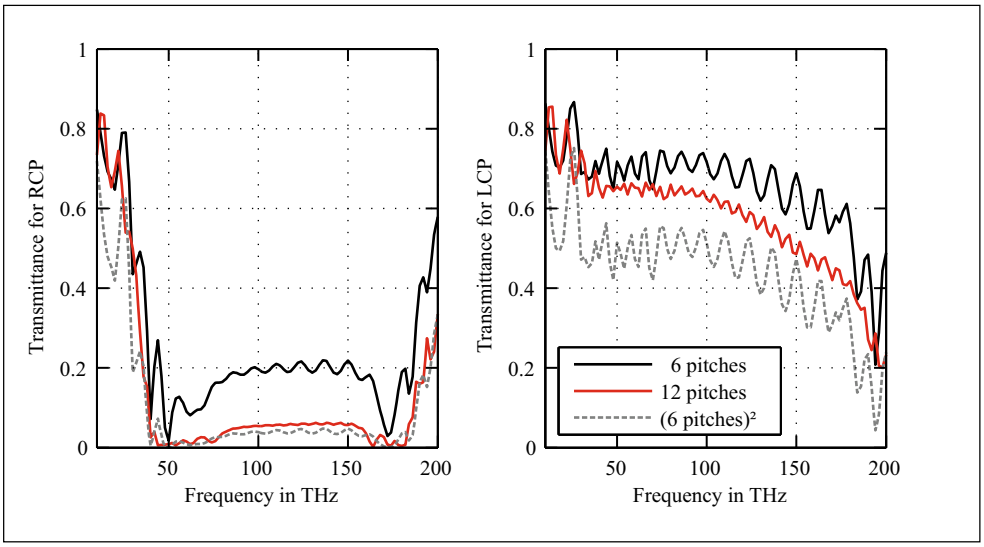

Fig. 5. The transmittance spectra for RCP and LCP are shown for 6 and 12 pitches in black and red, respectively. The same geometrical parameters were used as before with a taper ratio of $r_2 / r_H = 4$. The dashed, gray curves are a rough approximation for 12 pitches that is obtained by squaring the transmittance spectra for 6 pitches.

4. Conclusions

In conclusion, we have demonstrated that $N = 3$ helices, if arranged in a hexagonal lattice, show strictly zero circular polarization conversions. Furthermore, we have shown that, just as in the case of $N = 4$ helices, losses are essential to obtain circular dichroism. To obtain these results, we have used a different reasoning than previously for $N = 4$ helices, namely one based on reciprocity. We emphasize again at this point, that our reasoning holds true not only for N-helical structures, but for all reciprocal structures that carry an overall three- or four-fold rotational symmetry when only zeroth diffraction orders are present.

Our numerical calculations show a slightly worse performance for $N = 3$ helices compared to the case of $N = 4$, which we assign to the smaller gold volume filling fraction and thus smaller effective absorption. By varying the helix radius, we have demonstrated that bandwidth and extinction ratio cannot be optimized simultaneously for untapered $N = 3$ helices. Therefore, we have suggested a novel design, namely tapered $N = 3$ helices on a hexagonal lattice. This

design shows both, improved extinction ratio and larger bandwidth with increasing taper ratio.

While the achievable values for the extinction ratio are still orders of magnitude worse than what is feasible for linear wire-grid polarizers, the observed trend unequivocally shows that with more complex designs polarization-conserving helical structures with strong circular dichroism over an unmatched bandwidth come into reach.

Acknowledgments

We acknowledge support by the Deutsche Forschungsgemeinschaft (DFG), the Open Access Publishing Fund of Karlsruhe Institute of Technology, the State of Baden-Wrttemberg, the Karlsruhe Institute of Technology (KIT) through the DFG-Center for Functional Nanostructures (CFN) within subprojects A 1.4 and A 1.5, and by the Einstein Foundation Berlin through ECMath within subprojects SE6 and OT5. The PhD education of J. K. is embedded in the Karlsruhe School of Optics & Photonics (KSOP).